View metadata, citation and similar papers at core.ac.uk

brought to you by CORE

provided by University of Liverpool Repository

Journal Pre-Proof

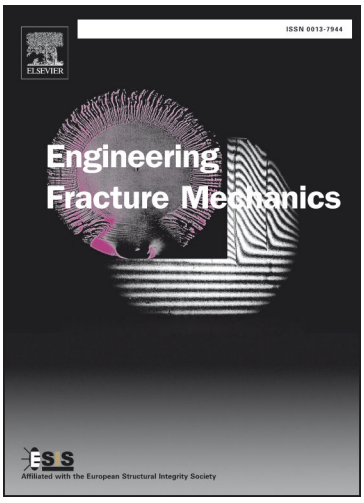

Determination of the crack initiation stress, elastic modulus and ultimate crack length in TPBT concrete beams based on shear deformation theory

Pu Jia, Lang Li, Jiangfeng Dong, Qingyuan Wang, Zhongwei Guan

PII: S0013-7944(19)30378-9
DOI: https://doi.org/10.1016/j.engfracmech.2019.106572
Reference: EFM 106572

To appear in: *Engineering Fracture Mechanics*

Received Date: 21 March 2019
Revised Date: 13 June 2019
Accepted Date: 17 July 2019

Please cite this article as: Jia, P., Li, L., Dong, J., Wang, Q., Guan, Z., Determination of the crack initiation stress, elastic modulus and ultimate crack length in TPBT concrete beams based on shear deformation theory, *Engineering Fracture Mechanics* (2019), doi: https://doi.org/10.1016/j.engfracmech.2019.106572

This is a PDF file of an article that has undergone enhancements after acceptance, such as the addition of a cover page and metadata, and formatting for readability, but it is not yet the definitive version of record. This version will undergo additional copyediting, typesetting and review before it is published in its final form, but we are providing this version to give early visibility of the article. Please note that, during the production process, errors may be discovered which could affect the content, and all legal disclaimers that apply to the journal pertain.

© 2019 Published by Elsevier Ltd.

JOURNAL PRE-PROOF

Determination of the crack initiation stress, elastic modulus and ultimate crack length in TPBT concrete beams based on shear deformation theory

Pu Jia[a,d], Lang Li[b], Jiangfeng Dong[b], Qingyuan Wang[b,c,*], Zhongwei Guan[c,d,*]

a MOE Key Laboratory of Deep Earth Science & Engineering, Institute for Disaster Management & Reconstruction, Sichuan University, Chengdu 610207, PR China

b Failure Mechanics & Engineering Disaster Prevention and Mitigation Key Laboratory of Sichuan Province, College of Architecture & Environment, Sichuan University, Chengdu 610065, PR China

c School of Mechanical Engineering, Chengdu University, Chengdu 610106, PR China

d School of Engineering, University of Liverpool, Liverpool L69 3GQ, UK

[*] Corresponding author: Qingyuan Wang, Tel/Fax +862885406919 Email wangqy@scu.edu.cn

[*] Corresponding author: Zhongwei Guan, Tel/Fax +441517945210 Email zguan@liv.ac.uk

Note: the surnames of the authors are underlined.

Abstract

Shear deformation theory was adopted in this research to analyse the crack initiation stress occurred in the three-point bending test (TPBT) on concrete beams. For TPBT concrete beams with different spans, the influence of shear force on the maximum stress and mid-span deflection was analysed. The relationship of the crack initiation stress, the modulus of rupture and splitting tensile strength was also studied. It was found that the crack initiation stress was about 90 percent of the modulus of rupture provided by the ASTM, British and European codes, and it was 1.125 times of the splitting tensile strength. Experimental study on notched concrete beams was also undertaken to validate the analytical results. For notched concrete beams in TPBT, calculations of elastic modulus and ultimate crack length are presented.

Keywords: Crack initiation stress; Modulus of rupture; Shear deformation theory; Notched beam; Fracture process zone

1. Introduction

Crack is a vital issue for concrete which is one of the most widely used materials in civil engineering. Firstly, cracks may occur during the full life cycle of concrete members, e.g. curing and service period.

Nomenclature

A_1, B_1, C_1, D_1, G_1, A_2	coefficients in W_m and X_m	SDT	shear deformation theory
b, h, l	width, depth and span of the beam (mm)	t, t_c	crack opening width and the maximum crack opening width in FPZ (mm)
CBT	classical beam theory	u_x, u_z	horizontal and vertical displacement (mm)
CMOD	crack mouth opening displacement (mm)	u_{zu}	mid-span deflection when a unit load (1000 N) is applied in TPBT (mm)
E	elastic modulus (GPa)	u_0, w_0	displacement along the axe x and z (mm)
f_{cr}	crack initiation stress (MPa)	U_m, W_m, X_m	Fourier coefficients in u_0, w_0, $\varphi(x)$
f_r	flexural strength provided by ASTM, British and European codes (MPa)	U	coefficient in u_{CR}
f_{spt}	splitting tensile strength (MPa)	u, u_{NC}, u_{CR}	total deflection, deflection caused by flexure and caused by crack propagation (mm)
FPZ	fracture process zone	w_c	maximum crack opening width in the fictious crack (mm)
g_i (i=1,2,3,4)	coefficients in σ_x, τ_{xz} and u_z	α, β	crack to depth ratio and span to depth ratio of the notched beam
G_F	fracture energy ($\mathrm{J/mm^2}$)	α_s, β_s, α_F	coefficients in bi-linear softening model
h_1, h_2, h_3, H_2,	depth of the compression, tension, FPZ and vital tension zones (mm)	δ	Dirac delta function
l_c, l_{cr}	crack propagation length and critical crack propagation length (mm)	ε_x, γ_{xz}	longitudinal strain and shear strain
m	mode number	ε_{x0}, κ_x, η_x	parameters in ε_x and γ_{xz}
N, M, S, Q	internal force (N) and moment (N · mm)	λ	coefficient in series sum form of u_0, w_0, $\varphi(x)$ and q
P	concentrated force applied at mid-span of the beam (N)	v	Poisson's ratio
P_{cr}, P_{ul}	crack initiation load and ultimate load in TPBT (N)	σ_{um}	maximum nominal stress when a unit load (1000 N) is applied (MPa)
q	arbitrary vertical load along the beam in SDT (N/mm)	$\varphi(x)$	rotation of the neutral layer
q_m	Fourier coefficients in q	$\psi(z)$	non-linear variation across the thickness

For fresh concrete, Ghourchian et al. [1] studied the performance of different passive methods in mitigation of plastic shrinkage cracks. By applying 3D X-ray CT, Shields et al. [2] investigated the crack sources of concrete in freeze-thaw condition. It was found that aggregate and matrix cracks were more prominent in concrete with a saturation degree of 95% and 100%. A large majority of researches were also conducted on the crack behaviour and failure of concrete members under different loading conditions. Moreover, crack is a basic precondition for investigating self-healing concrete, one of the post popular research subjects in the cement-based materials [3–

5]. Secondly, cracks provide a path for water and ionic species to penetrate the concrete, which may significantly compromise the service life of concrete members.

It is generally believed that crack initiation and growth and fracture properties of concrete are closely related to its tensile strength. In the direct tensile testing, dog-bone shaped, unnotched and notched prism or cylinder specimens with different geometries and gripping systems are used, and there is still lack of a standardized method to investigate the tensile behaviour of concrete by tensile testing [6–10]. In addition, the gripping specimens in direct tensile tests may encounter with problems of load eccentricity and stress nonuniformity [11]. As a consequence, the direct uniaxial tensile tests of concrete, which are difficult to be carried out, have been given little attention by researchers [11,12].

The indirect tensile tests on concrete, i.e. three-point bending test, compact tension test, and wedge splitting test, are adopted extensively in concrete fracture investigations [13]. As TPBT can be stably performed on notched beams, TPBT is commonly used in concrete fracture tests [14–16]. Based on TPBT, various models using nonlinear fracture mechanics of concrete, such as two-parameter fracture model, size-effect model, effective crack model, double-K and double-G fracture model, were proposed and improved by many researchers. Through measuring the load, deflection and crack mouth opening displacement (CMOD), some important fracture parameters could be obtained [17–19].

In TPBT, flexure strength (i.e. modulus of rupture) is frequently calculated based on the classical bending theory (CBT) [20–23]. Indeed, it is crucial to determine flexure strength correctly, due to a large number of flexural members used in engineering applications. If uncertainty occurs in determining flexure strength, both allowable stress design and limit state design in structural engineering can be affected [24].

In the determination of flexural strength, it is imperative to note that there are two basic assumptions in the bending theory. The first one is that all cross section of the beam remains plane and perpendicular to the longitudinal axis during deformation. The second one is that the small lateral strain due to the Poisson's effect is negligible, i.e. the cross-section retains its original shape [25]. Hence, the classical beam theory does not apply to model transverse shear deformation and is only appropriate for a shear bending beam with a high aspect ratio where shear deformation is not prominent.

However, in three-point bending fracture tests of notched beams, the recommended span to depth ratio is 4 [13,26,27]. Moreover, a smaller ratio, i.e. 3, is adopted in the determination of modulus of rupture in ASTM [28],

British and European standards [29,30]. For these deep beams, the basic assumptions made in the CBT may be invalid as the effect of transverse stress on cross-sectional deformation is not negligible. The CBT may bring a large relative error in the tensile stress calculations and the issues on how to accurately analyse the related problems need to be addressed.

A similar situation appears in the laminated composite and sandwich structures, which have superior properties and reliability and have been extensively utilized in naval, automobile and civil engineering industries [31]. For these structures, transverse shear deformation is a major issue in the mechanical analysis due to their relatively low value of shear modulus as compared to traditional materials [32]. However, the CBT does not apply to model transverse shear deformations and is not appropriate for these laminated composite structures. Hence, a lot of work has been carried out to estimate the transverse shear deformations correctly and efficiently for design purpose.

Shear deformation theory (SDT) is proposed and has been widely adopted in the static and dynamic analysis of laminated beams, plates, and shells [33–36]. By adopting the layerwise SDT, Shimpi and Ghugal [36] presented the analysis of two-layered cross-ply laminated beams. A general framework for the free vibration analysis of thick laminated doubly-curved panels and shells was provided by Viola et al. [37].

According to the generalized unified formulation [31], there are mainly three well-known equivalent single layer (ESL) shear deformation theories, i.e. the classical lamination theory (CLT), the first order shear deformation theory (FSDT) and the higher-order shear deformation theory (HSDT). The HSDT assumes quadratic, cubic or higher (trigonometric) variations of surface-parallel displacements through the entire thickness of laminate to model the transversal shear deformation.

Based on the trigonometric SDT, extensive investigations have been carried out on composite beams and plates [38,39]. For example, Zenkour [40] studied the bending behaviour of a simply supported rectangle functionally graded material plate. By means of the refined trigonometric SDT, Tounsi et al. [41] investigated the thermoelastic bending of functional graded sandwich plates. Utilizing the trigonometric SDT, Arya et al. [32] predicted displacements and stresses for symmetric cross-ply laminated beams. The predictions result in high accuracy, even for the beam with a small length to depth ratio.

There has been extensive research on flexural and fracture properties of concrete beams in TPBT and the applications of SDT on laminated members. However, up to date the influence of shear force on nominal stress

distribution in TPBT concrete beams has not been given enough attention. The true maximum nominal stress occurred in the crack initiation and propagation has also long been neglected. Hence, in the current study, the basic theory of trigonometric SDT is adopted to analyse the stress and deformation of concrete beams in TPBT. Based on the experimental results of notched concrete beams in TPBT, the effect of shear force on the crack initiation stress and flexural strength is studied here. In addition, the relationships of the splitting tensile strength, the crack initiation stress and the flexural strength provided by the ASTM, British and European codes [28–30] are discussed. Furthermore, the elastic modulus and critical crack propagation length in TPBT of notched concrete beams are determined. The results of this paper can be contributed to the more reasonable crack and fracture calculations and rational allowable stress design and limit state design of concrete structures.

2. Development of the proposed theory

2.1. Shear deformation theory

Consider a rectangular beam with a span *l*, width *b* and depth *h*, subjected to a distributed load, *q*, as shown in Fig. 1. In the coordinate system, the *x*-axis is at the centre of the beam along its longitudinal direction and the *z*-axis is perpendicular to it. The longitudinal and transverse displacements at any point (*x*, *z*) in the beam can be written as [32,40]:

$$u_x(x,z) = u_0(x) - z\cdot\partial_x w_0(x) + \psi(z)\cdot\varphi(x)$$
$$u_z(x,z) = w_0(x) \qquad \text{(1a-b)}$$

Where u_0 and w_0 are the displacements along *x* and *z* axes respectively, $\varphi(x)$ is a rotation about the *y*-axis which is perpendicular to the *x*-*z* plane.

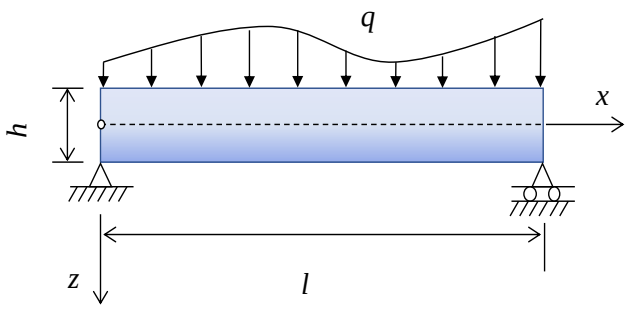

Fig. 1. The geometry of a rectangular beam.

Using the trigonometric shear deformation theory, there is $\psi(z) = h/\pi\cdot\sin(z\pi/h)$. Here, the trigonometric sine

term, $\psi(z)$, represents the non-linear variation across the thickness and *h* is the beam depth.

The longitudinal strain and shear strains compatible with the displacement are

$$\varepsilon_x = \partial_x u_0(x) - z \cdot \partial_x^2 w_0(x) + \psi(z) \cdot \partial_x \varphi(x)$$
$$\gamma_{xz} = \partial_z \psi(z) \cdot \varphi(x) \tag{2a-b}$$

The governing equations of equilibrium associated with the displacement functions can be derived by using the principle of virtual displacements. These variation consistent equations are

$$\partial_x N = 0$$
$$\partial_x^2 M + q = 0 \tag{3a-c}$$
$$\partial_x S - Q = 0$$

where *N* and *M* are the basic components of stress resultant and stress couples, *S* is an additional stress couple associated with the transversal shear effects, *Q* is transversal shear stress resultant. The resultant force and moment can be obtained by $[N, M, S] = \int_{-h/2}^{h/2} \sigma_x [1, z, \psi(z)] d_z$ and $Q = \int_{-h/2}^{h/2} \tau_{xz} \cdot \partial_z \psi(z) d_z$, where $\sigma_x = E\varepsilon_x$ and $\tau_{xz} = \gamma_{xz} E / (2(1+\nu))$, *E* and *v* are the elastic modulus and Poisson's ratio respectively.

2.2 The exact solutions of SDT in TPBT

To solve the present problem, the following solution forms based on the displacement functions, which satisfy the simply supported boundary conditions, are adopted.

$$u_0(x) = \sum_{m=1}^{\infty} U_m cos(\lambda x)$$
$$w_0(x) = \sum_{m=1}^{\infty} W_m \sin(\lambda x) \tag{4a-c}$$
$$\varphi(x) = \sum_{m=1}^{\infty} X_m \cos(\lambda x)$$

where $\lambda = m\pi / l$, U_m, W_m and X_m are arbitrary parameters to be determined, and *m* is mode number.

Similar to the displacement functions, the external force is expressed in the form of a trigonometric series

$$q(x) = \sum_{m=1}^{\infty} q_m \sin(\lambda x) \tag{5}$$

where q_m is the Fourier coefficients which can be calculated by $q_m = 2/l \cdot \int_0^l q(x) \sin(\lambda x) dx$. For a concentrated load *P* applied at the mid-span in TPBT, it can be expressed as $q(x) = P / b \cdot \delta(x - l/2)$, where $\delta(x - l/2)$ is the Dirac delta function.

By substituting Eqs. (2), (4) and (5) into Eq. (3), parameters U_m, W_m and X_m can be solved, which are expressed as follows.

$$\begin{aligned} U_m &= 0 \\ W_m &= [A_1 P\beta^3/(Eb\pi^4)]\cdot sin(m\pi/2)[B_1\beta^2 + C_1 m^2\pi^2(1+\nu)]/[D_1 m^4\beta^2 + G_1 m^6\pi^2(1+\nu)] \\ &= W_m^{'}\cdot P/(Eb) \\ X_m &= [A_2 P\beta^2/(Eb\pi h)]\cdot[sin(m\pi/2)(1+\nu)]/[D_1 m\beta^2 + G_1 m^3\pi^2(1+\nu)] = X_m^{'}\cdot P/(Eb) \end{aligned} \tag{6a-c}$$

where $\beta = l/h$ is the span-depth ratio, A_1, B_1, C_1, D_1, G_1 and A_2 are the coefficients independent of the span and depth. The computed results of A_1, B_1, C_1, D_1, G_1 and A_2 are shown in Appendix A.

In this case, for a beam specimen with a span of l and depth of h, the longitudinal stress and deflection at point (x, z) can be determined by the following equations.

$$\sigma_x(l,h,x,z) = P/b\cdot[g_1(l,h,x)\cdot z + g_2(l,h,x)\cdot(h/\pi)\sin(\pi z/h)] \tag{7}$$

$$u_z(l,h,x,z) = P/(Eb)\cdot g_3(l,h,x) \tag{8}$$

where

$$\begin{aligned} g_1(l,h,x) &= \sum_{m=1}^{\infty}\lambda^2 W_m^{'} sin(\lambda x) \\ g_2(l,h,x) &= -\sum_{m=1}^{\infty}\lambda X_m^{'} sin(\lambda x) \\ g_3(l,h,x) &= \sum_{m=1}^{\infty} W_m^{'} sin(\lambda x) \end{aligned} \tag{9a-b}$$

2.3. Determination of E in TPBT of a notched concrete beam

For concrete, its elastic modulus is a basic material property, which is mainly determined by compression testing of the cylinder. In fact, the deflection in TPBT is closely related to the elastic modulus. However, with the influence of both the shear force and initial notch on the deflection, the accurate calculation of elastic modulus in bending fracture tests is difficult. Here, an attempt was made to obtain the elastic modulus by utilizing the measured data in bending tests based on the SDT.

For the pre-notched beams in TPBT, the mid-span deflection at the ultimate load is caused by the shear dominated bending (u_{NC}) together with the crack opening (u_{CR}). Hence, it can be expressed as $u_{ul} = u_{NC} + u_{CR} = u_{NC} + P/(Eb)\cdot U(\alpha,\beta)$, where α and β are the notch to depth ratio and span to depth ratio, respectively. As to the coefficient item of $U(\alpha,\beta)$, different empirical models are proposed [26,42–44].

For the notched beam with a span to depth ratio of 4, $U(\alpha,\beta)$ can be computed by

$$U(\alpha,\beta)=(3\beta^2/2)[\alpha/(1-\alpha)]^2(5.58-19.57\alpha+36.82\alpha^2-34.94\alpha^3+12.77\alpha^4) \quad \text{(Tada [26], 10a)}$$

$$U(\alpha,\beta)=\beta^2/(1-\alpha)^2\cdot(1.193-1.980\alpha+4.478\alpha^2-4.443\alpha^3+1.739\alpha^4) \quad \text{(Underwood [42], 10b)}$$

$$\begin{aligned}U(\alpha,\beta)=4.5\beta^2\{&-0.3645\alpha^5+1.326\alpha^4-2.71\alpha^3+3.874\alpha^2-8.614\alpha\\&-2.268+6.018\ln(1+2\alpha)-1.015\ln(1-\alpha)\\&+(2.829\alpha^2-4.437\alpha+2.268)/[(1+2\alpha)(1-\alpha)^2]\}\end{aligned} \quad \text{(Wu [43], 10c)}$$

Moreover, Guinea et al. [44] proposed a model, which is valid for notched beams with a span to depth ratio larger than 2.5, which can be expressed as

$$\begin{aligned}U(\alpha,\beta)=72\{&[\alpha(-7.8224+6.3904\beta-0.6327\beta^2)/432+\alpha^2(11-0.88\beta)(1.24-0.14\beta)/864\\&-\alpha^3(-1.24+0.14\beta)^2/432+2.65\alpha\beta(-4.64+0.13\beta)/[512(1-\alpha)]\\&+\alpha(2.65\beta)^2(2-\alpha)/[512(1-\alpha)^2]-\alpha(16.48+45.19\beta)^2/[82944(1+3\alpha)]\}\end{aligned} \quad \text{(Guinea [44], 10d)}$$

The equations of those models are indeed complex and therefore, the u_{ul}/u_{NC} is calculated and fitted in a form of exponential function, as shown in Fig. 2. For a notched concrete beam with a span to depth ratio of 3 or 4 and a notch to depth ratio between 0.1 and 0.8, its elastic modulus can be obtained by

$$\begin{aligned}E&=P_{ul}/(u_{ul}b)\cdot g_3(l,h,x)\cdot u_{ul}/u_{NC}\\&=P_{ul}/(u_{ul}b)\cdot(4\beta^2+0.78\beta)\cdot\exp(0.4177-2.2433\alpha+6.7675\alpha^2)\end{aligned} \quad (11)$$

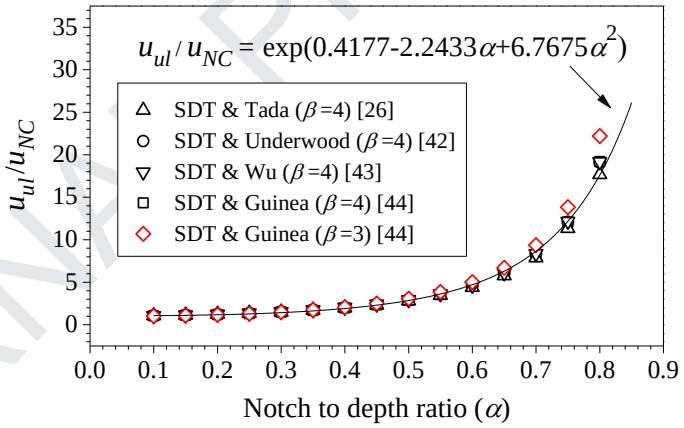

Fig. 2 The relationship between u_{ul}/u_{NC} and α (β = 3, 4).

2.4. Stress distribution in the critical cross section

As concrete is a material which has different properties in tension and compression, its neutral axis will shift away from the tensile side after the crack formation, accompanied by the redistribution of stresses. Moreover, as a quasi-brittle material, a large and variable size of damage zone also exists ahead of the macro-crack. This damage zone is known as the fracture process zone (FPZ) and has the capacity to transfer the cohesive stress

across the crack faces which decreases with increasing deformation [13]. In this study, the cohesive stress along FPZ is assumed to be linear over the micro-cracks and the bilinear softening traction-separation law is adopted, as shown in Fig. 3.

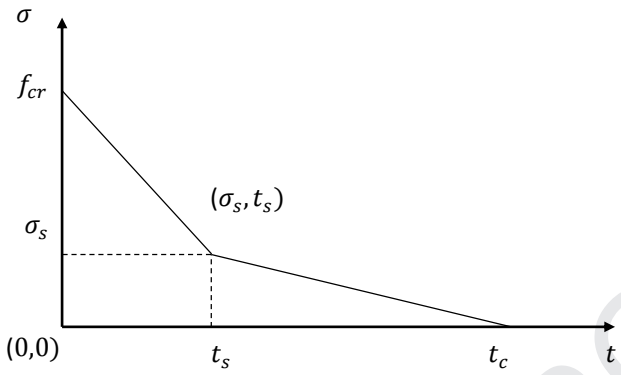

Fig. 3. The distribution of cohesive stress along FPZ.

The cohesive stress can be expressed as

$$\begin{aligned} &\sigma = f_{cr} - (f_{cr} - \sigma_s)t / t_s, \quad 0 \le t \le t_s \\ &\sigma = \sigma_s (t_c - t) / (t_c - t_s), \quad t_s \le t \le t_c \\ &\sigma = 0, \quad t_c \le t \end{aligned} \tag{12a-c}$$

where t is the crack opening width. The maximum crack opening displacement in the FPZ, t_c, can be calculated by $t_c = \alpha_F G_F / f_{cr}$, where $\alpha_F = 9 - d_a$. Here, G_F and d_a are the fracture energy and maximum size of aggregate respectively.

The value of a kink point in a non-dimensional form is $\alpha_s = \sigma_s / f_{cr}$ and $\beta_s = t_s / t_c$ respectively. The coefficients, α_s and β_s, can be determined by $\alpha_s = (2 - f_{cr} \cdot CTOD_c / G_F) / \alpha_F$ and $\beta_s = t_s / CTOD_c = 1$, where $CTOD_c$ is the critical crack tip opening displacement.

As aforementioned, after formation of a crack, there are three stress zones, i.e. the tension, compression and fracture progress zones, along with the mid-span cross-section. The stresses redistributed at ultimate load are shown in Fig. 4. It should be mentioned that the tensile zone (h_2), corresponding to the crack initiation stress f_{cr}, is assumed to be a part of the vital tensile zone with a depth of H_2. This can be regarded as the consequence of the formation of cohesive stress zone. If this hypothesis does not conform to reality, the results of h_2 and H_2 will be equal with each other and they have no influence on the calculation of critical crack propagation length.

The equilibrium and geometry equations, which are required to determine the size of stress zones, are given by

$$\begin{aligned} &N_1 + N_2 + N_3 = 0 \\ &M_1 + M_2 + M_3 = P_{ul} \cdot l / (4b) \\ &h_1 + h_2 + h_3 = h \\ &f_{cr} = \sigma_x(l, H_2, l/2, h_2) \end{aligned} \tag{13a-d}$$

where P_{ul} is the ultimate load, the subscript *1*, *2* and *3* are related to the compressive, tensile and fracture progress zones, respectively.

It should be noted that the coefficient items g_1 and g_2 in Eq. (9) are described in the manner of series summation, which leads to great difficulty in solving equation set (13). Consequently, results of the series summation are fitted using an exponential function. The detailed fitting expressions are shown in Appendix B.

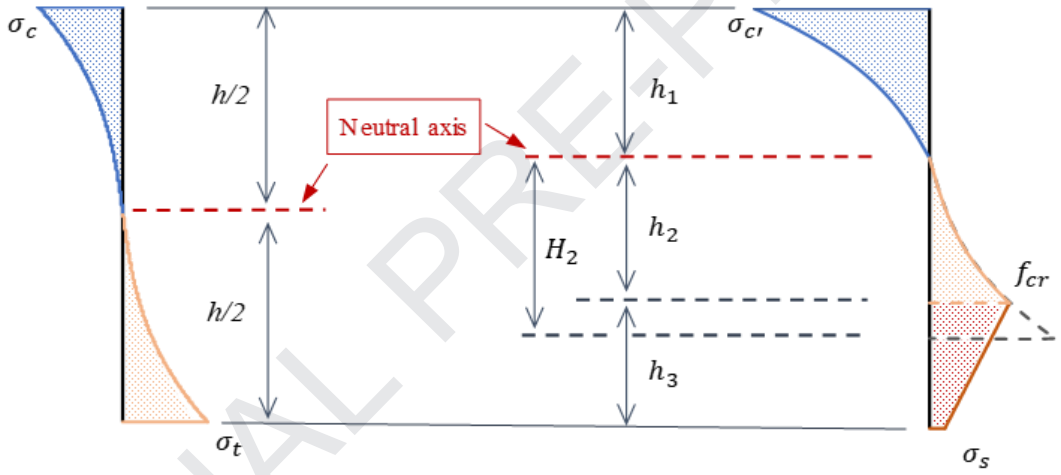

Fig. 4. The stress distribution along the critical cross-section at mid-span.

3. Experimental setup for validation of the theory

In this study, the notched concrete beams with a span to depth ratio of 3 and cylinders were selected to prove the validity of SDT in the concrete fracture test. In each type of tests, three repeated tests were carried out to obtain the corresponding average results. The detailed experimental setup is shown in Fig. 5. Both the calculated elastic modulus and crack propagation length, based on SDT, are compared with the experimental ones. By determining the crack initiation load and ultimate load in TPBT, i.e. P_{cr} and P_{ul}, the relationship between the cracking stress and traditional modulus of rupture are analysed.

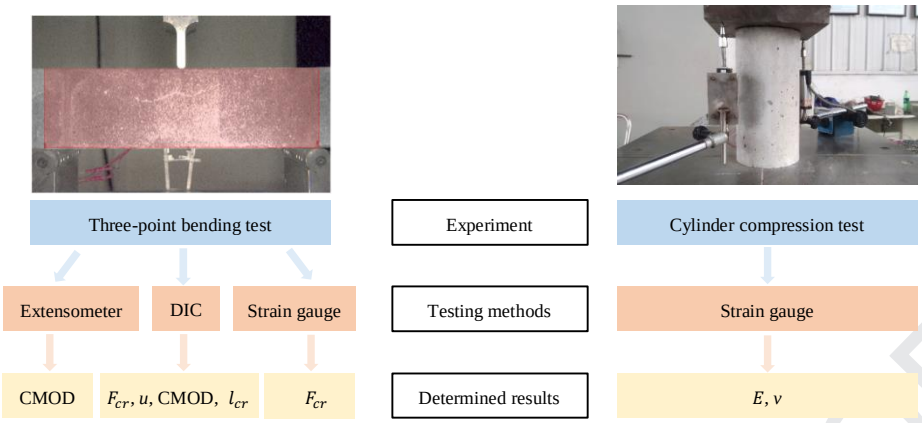

Fig. 5. The experimental setup adopted in this study.

As the accurate determination of deflection is vital in this research, the digital image correlation (DIC) method was adopted. The displacement caused by the gap between the specimen and supports, which is the major error source in the deflection measurement, was also determined by the DIC method. In order to identify deformations clearly, the specimen surface was treated by creating a random, sprayed-on speckle pattern.

Both normal and basalt fibre concrete, whose mixture properties are listed in Table 1, were used to make the specimens. The notched beams are with a dimension of 100 mm×100 mm×400 mm, and a notch depth of 30 mm. The geometry of the notched beam is shown in Fig. 6. The cylinders are with a radius of 50 mm and a height of 200 mm. In TPBT, an electronic universal testing machine with a maximum capacity of 100 kN was employed. An extensometer was used to determine the crack mouth opening displacement (CMOD). For the cylinder compression test, a 2000 kN electro-hydraulic servo universal testing machine was utilized.

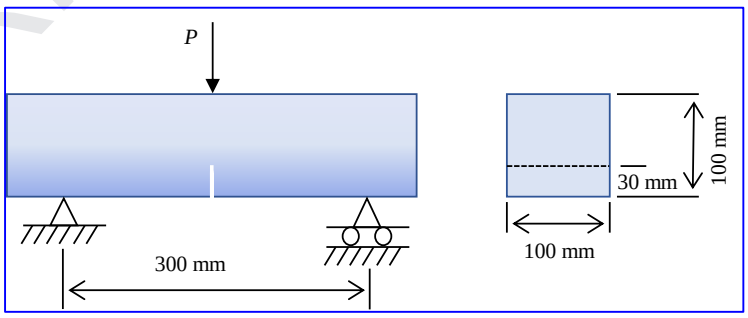

Fig. 6. The geometry of the notched beam.

Table 1

The concrete mixture properties (kg/m^3).

Specimen	Cement	NCA	RCA	Sand	Fly ash	Water	Fibre	S.P.
NC	440	620	620	610	110	165	0	1.1
FC	440	620	620	610	110	165	4	1.1

Note: NCA - natural coarse aggregate; RCA - recycled coarse aggregate; S.P. - superplasticizer.

4. Results and discussion

4.1 The maximum nominal stress and mid-span deflection based on SDT and CBT

Here, the stress distribution in a beam with a dimension of 300 mm×100 mm×100 mm is calculated by both SDT (Eq. 7) and $\sigma_{CBT}(z) = 3Plz/(bh^3)$. If a unit load of 1000 N is applied and a Poisson's ratio of 0.3 is adopted, the calculated stresses across the beam depth are plotted in Fig. 7. It is clear that, for the maximum nominal stress occurred at the point farthest away from the neutral axis, the one obtained by SDT is larger than the CBT one. For the beam with a span to depth ratio of 3, which is recommended in the ASTM, British and European codes [28–30], the modulus of rupture computed by SDT is even 49.3% larger than the CBT one. It indicates that, for TPBT beams made of brittle material with a low span to depth ratio, the CBT significantly underestimates the maximum nominal stress on the cross-sectional area of a beam.

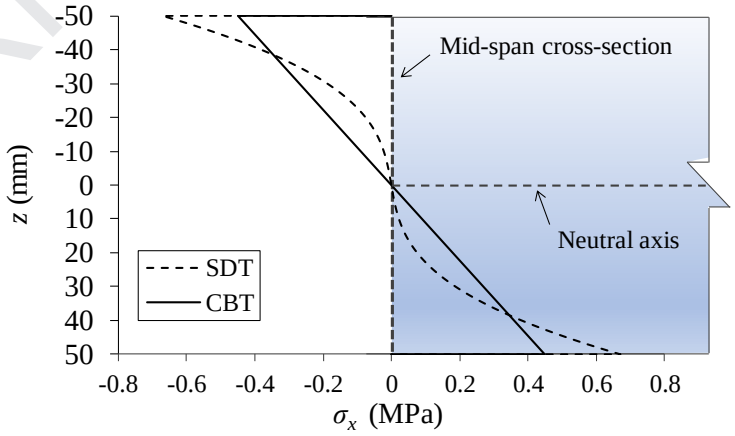

Fig. 7. The stress distribution in the mid-span cross-section based on CBT and SDT (a unit load P=1000N is applied at mid-span).

Subsequently, for beams with the same cross-section (100 mm×100 mm), the effects of the span on the deviation of the maximum nominal stress and mid-span deflection are considered. For a unit load of 1000 N being applied, the corresponding maximum nominal stress and deflection at mid-span ($x = l/2$) are defined as the unit maximum nominal stress (σ_{um}) and unit mid-span deflection (u_{zu}). They can be obtained by setting $P = 1000\text{N}$, $b = h = 2z = 100\text{mm}$ in Eqs. (7) and (8) or $\sigma_{CBT}(z) = 3Plz/(bh^3)$ and $u_{CBT}(z) = Pl^3/(4Ebh^3)$. An elastic modulus of 20 GPa is adopted in the deflection calculation.

A span range of 300 – 1200 mm is considered. The calculated unit maximum nominal stress and unit mid-span deflection based on CBT and SDT are listed in Table 2. The subscripts 'CBT' and 'SDT' mean the results are based on CBT and SDT respectively. The deviation and the relative deviation are defined as $\sigma_{um-SDT} - \sigma_{um-CBT}$ (or $u_{zu-SDT} - u_{zu-CBT}$) and $(\sigma_{um-SDT} - \sigma_{um-CBT})/\sigma_{um-SDT}$ (or $(u_{zu-SDT} - u_{zu-CBT})/u_{zu-SDT}$), respectively. The calculated derivations of the unit maximum nominal stress and unit deflection are shown in Fig. 8.

Table 2

The unit maximum nominal stress and mid-span deflection of beams with a cross-section of 100 mm×100 mm.

Span (mm)	300	400	500	600	700	800	900	1000	1100	1200
σ_{um-CBT} (MPa)	0.45	0.6	0.75	0.9	1.05	1.2	1.35	1.5	1.65	1.8
σ_{um-SDT} (MPa)	0.67	0.82	0.97	1.12	1.27	1.42	1.57	1.72	1.87	2.01
u_{zu-CBT} (μm)	3.38	8	15.63	27	42.88	64	91.13	125	166.38	216
u_{zu-SDT} (μm)	4.5	9.51	17.52	29.29	45.55	67.07	94.58	128.85	170.61	220.63

For the maximum stress, the derivation declines linearly with the increase in span, whilst the relative deviation has a large decrease in a nonlinear fashion for the span less than 600 mm, which can be regarded as the result of the significant increase in σ_{um-SDT}. For example, for beams with a span from 300 to 1200 mm, the relative deviation is dropped from 0.33 to 0.11. However, the high relative deviation, which is still larger than 0.1 for the beam with a span of 1200 mm, indicates a clear difference between the stresses computed by SDT and CBT.

Different from the trend of the stress derivation, the mid-span deflection derivation increases with the span linearly. In the TPBT, the deformation is caused by both the inner bending stress and shear stress and therefore, this derivation can be deemed as the displacement induced by the shear stress independently. Moreover, this part of the deformation can be calculated by $0.78Pl/(Ebh)$, which is based on the virtual work principle. The deviations are almost equal to the virtual work principle ones, as shown in Fig. 8(b). However, its relative

counterpart decreases sharply for beams with a span less than 600 mm. For the beam with a span larger than 550 mm, its relative deflection deviation is smaller than 0.1. With respect to the stress one, the deflection difference is less evident. Especially, for the specimen with a span of 300 mm, its relative deviation in the maximum stress and mid-span deflection is 0.33 and 0.25 respectively. It is conceivable to conclude that the influence of transverse shear deformations should be taken into consideration for the beams studied in this paper.

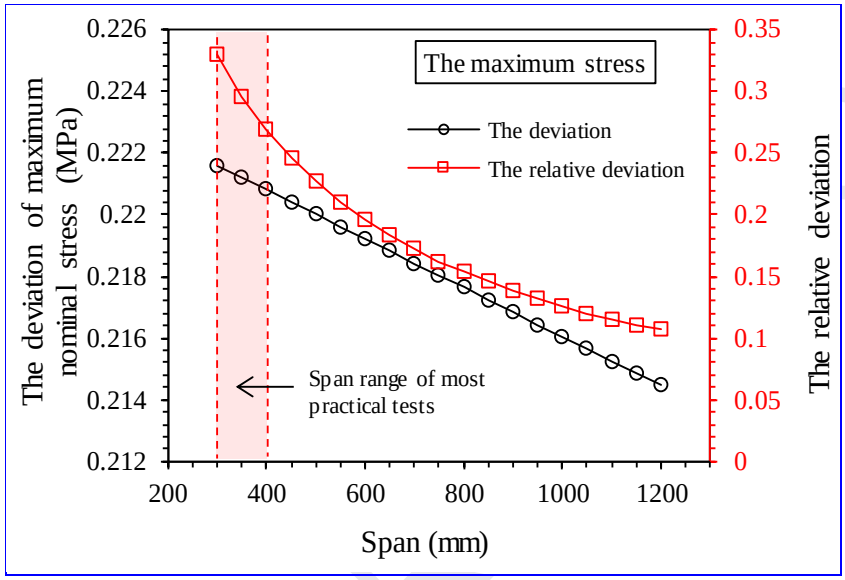

(a)

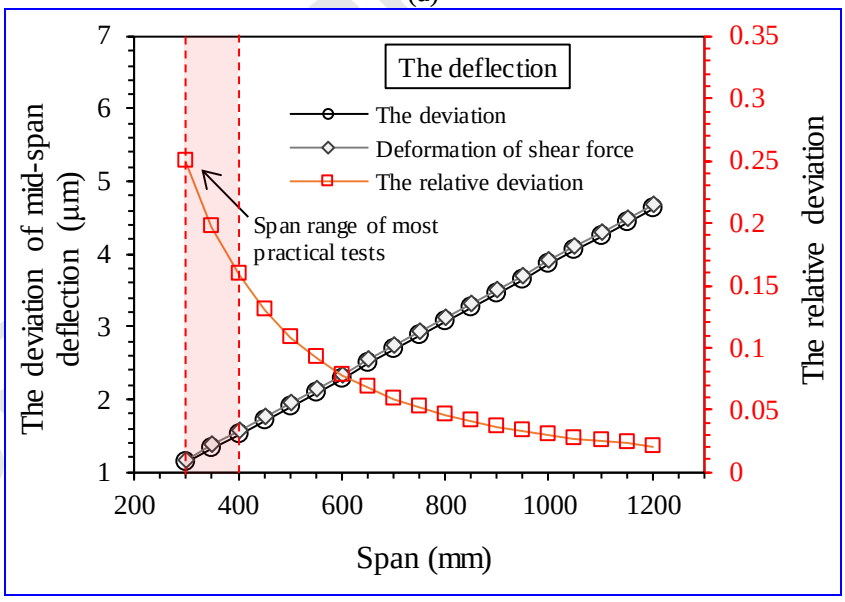

(b)

Fig. 8. The influence of span on the deviation: (a) the maximum stress; (b) the deflection.

4.2 The elastic modulus

Based on the proposed equation (11), the elastic moduli calculated are plotted in Fig. 9. ND2 and ND5 are the specimens adopted in [45] with a notch to depth ratio of 0.2 and 0.5 respectively. Notched concrete beams with

a dimension of 515×100×100 mm^3 were tested and a span to depth ratio of 4 was adopted [45]. The ultimate load and displacement used in the calculation are listed in Table. 3.

As shown in Fig. 9, the elastic modulus obtained by Eq. (11) is much closer to the experimental one in general. For specimens with a span to depth ratio of 3 and 4, the proposed equation can give results with a good correlation to the experimental measurements.

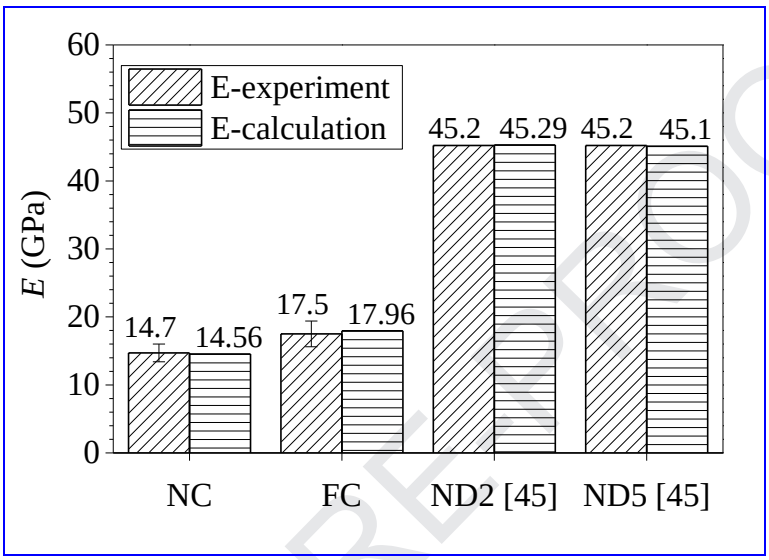

Fig. 9. The experimental and calculated results of elastic modulus.

Table 3

Test results of the notched beam.

Specimen	α	β	P_{ul} (N)	$CMOD_{ul}$ (mm)	u_{ul} (mm)	u_{NC} (mm)
NC	0.3	3	8302 ± 194	0.0447 ± 0.0008	0.059 ± 0.005	0.0415
FC	0.3	3	6405 ± 177	0.0444 ± 0.0008	0.056 ± 0.004	0.0396
ND2 [45]	0.2	4	8913	-	0.048	0.0374
ND5 [45]	0.5	4	3562	-	0.040	0.0150

4.3 The crack initiation stress and modulus of rupture

The modulus of rupture, f_r, is generally regarded as the flexural strength computed from the maximum bending moment [28–30]. For concrete beams, it can be regarded as a macroscopic value, which reflects the failure stress. However, the crack initiation stress, f_{cr}, is defined as the maximum tensile stress in the TPBT. It is the local stress at which the crack initiates and growths.

For determining such the stress, the crack initiation load need to be obtained firstly. In this study, both the strain gauges, which are attached beside the notch tip [14], and the DIC technique [46] are adopted to determine the crack initiation load. It is found that the crack loads of 5115 N and 3862 N for specimens NC and FC determined

by DIC are smaller than the strain gauge ones (5574 N and 4022 N). This may be related to the average strain, not the notch tip one, obtained by strain gauges.

As a result, the DIC results are utilized in the stress calculation. The obtained crack initiation stress and modulus of rupture are shown in Fig. 10. Clearly, there is a large difference between these stresses. In fact, the f_{r-CBT} in Fig. 10 is the modulus of rupture determined by the ASTM, British and European codes [28–30]. Consequently, attentions should be paid to their difference.

In the previous investigation conducted by Guo et al. [46], it was found that, for a notched concrete beam with a span to depth ratio of 3 and a notch to depth ratio of 0.2, the crack initiation load is equal to or larger than 60 percent of the peak load, i.e. $P_{cr} \geq 0.6P_{ul}$. The experimental results in this study are in consistent with this. Hence, for conservative calculations, it is reasonable to consider that P_{cr} equals 60 percent of P_{ul}. Moreover, taking account of the fact that the previous investigations were based on the classical beam theory, the crack initiation stress with better accuracy can be obtained by using shear deformation theory "SDT". Therefore, for a notched concrete beam with a span to depth ratio of 3 and a notch to depth ratio of 0.2 or 0.3, the stress can be determined by the following equation

$$f_{cr} = 0.6 f_r \cdot (\sigma_{un-SDT} / \sigma_{un-CBT}) \tag{14}$$

where f_r is the modulus of rupture, f_{cr} is the crack initiation stress, σ_{um-SDT} and σ_{um-CBT} is the unit maximum nominal stress calculated by shear deformation theory and classical beam theory respectively.

Based on the specimen dimensions in this study and Guo's results [46], it can be concluded that the crack initiation stress (by SDT) is about 89.5 percent of the modulus of rupture calculated by the ASTM, British and European codes [28–30]. It should be noted that, although a large difference occurs between the crack initiation load and the ultimate load, the calculated crack initiation stress based on SDT is close to the modulus of rupture computed by the ASTM, British and European codes [28–30], which are CBT based.

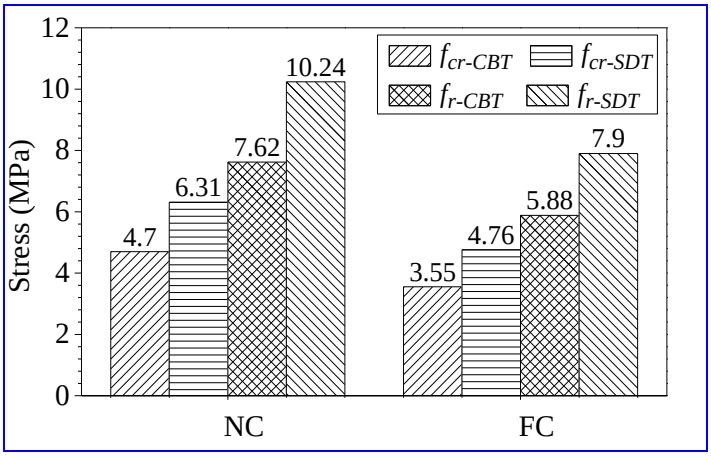

Fig. 10. The crack initiation stress and modulus of rupture calculated by SDT and CBT.

4.4 The critical crack propagation length

By solving equation set (13), the sizes of stress zones can be obtained, which are shown in Table 4. The DIC determined ones are also listed in Table 4. The fracture surface of failure specimens and determination of critical crack propagation length by DIC method is shown in Fig. 11 and Fig. 12 respectively.

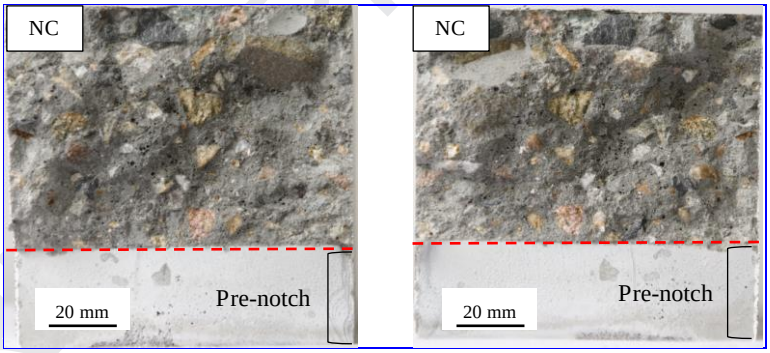

(a)

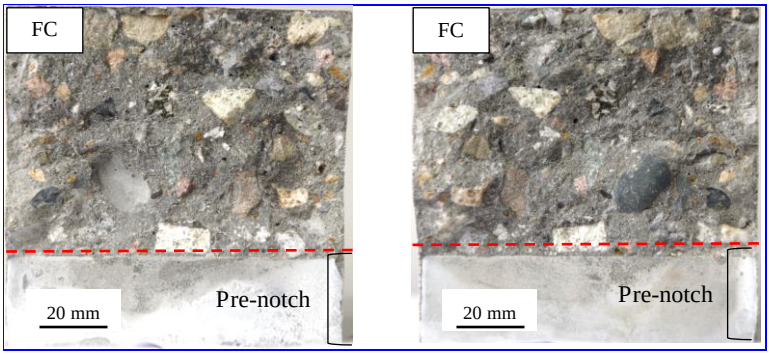

(b)

Fig. 11. The fracture surface of failure specimens: (a) NC; (b) FC.

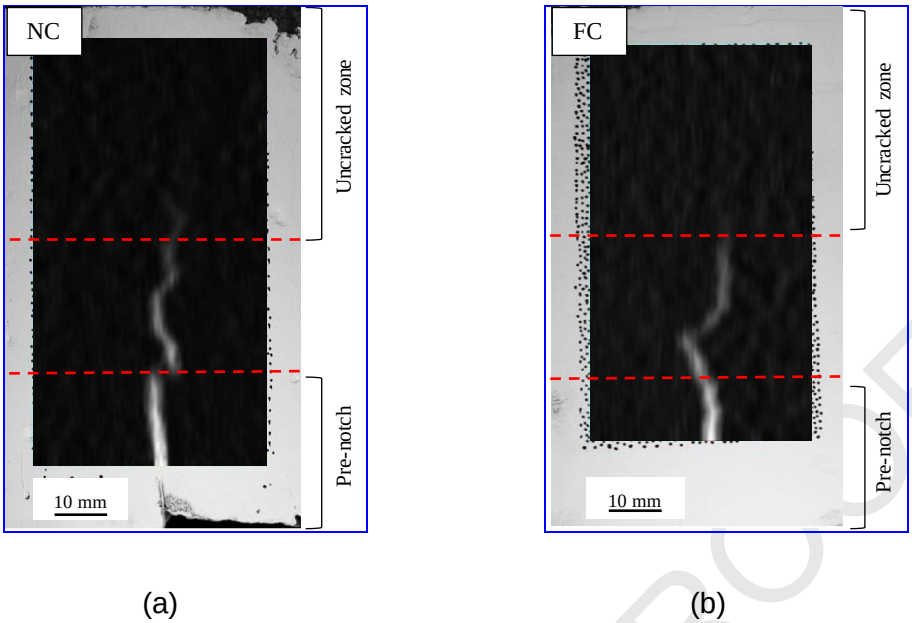

Fig. 12. The critical crack propagation length determined by DIC method: (a) NC; (b) FC.

Table 4

The calculated results of the size of different stress zones.

Specimen	h_1 (mm)	h_2 (mm)	h_3 (mm)	H_2 (mm)	h_{3-DIC} (mm)
NC	26.65	16.52	26.83	26.64	25.37 ± 1.23
FC	26.37	14.78	28.85	25.68	27.23 ± 1.57

For specimens NC and FC, their calculated crack propagation lengths are about 38.33 and 41.21 percent of the original depth, which are close to the ones determined by DIC, 36.25 and 38.9, respectively. The difference between the computed and experimental results of crack propagation length is small. This indicates that the crack initiation stress obtained by SDT is approaching to the real value. In addition, the results of h_2 and H_2 indicate that the appearance of crack has an influence on the stress distribution in tthe ension region, which are mentioned in the calculations of stress redistribution.

The ultimate crack propagation length based on f_{cr-CBT} and the CBT are then considered. However, in this case, the calculation has no solution. Moreover, the same situation occurs for the computation based on f_{cr-CBT} and stress distribution of SDT. Consequently, given the experimental ultimate load, the available f_{cr} and the corresponding crack propagation length are analysed, as shown in Fig. 13.

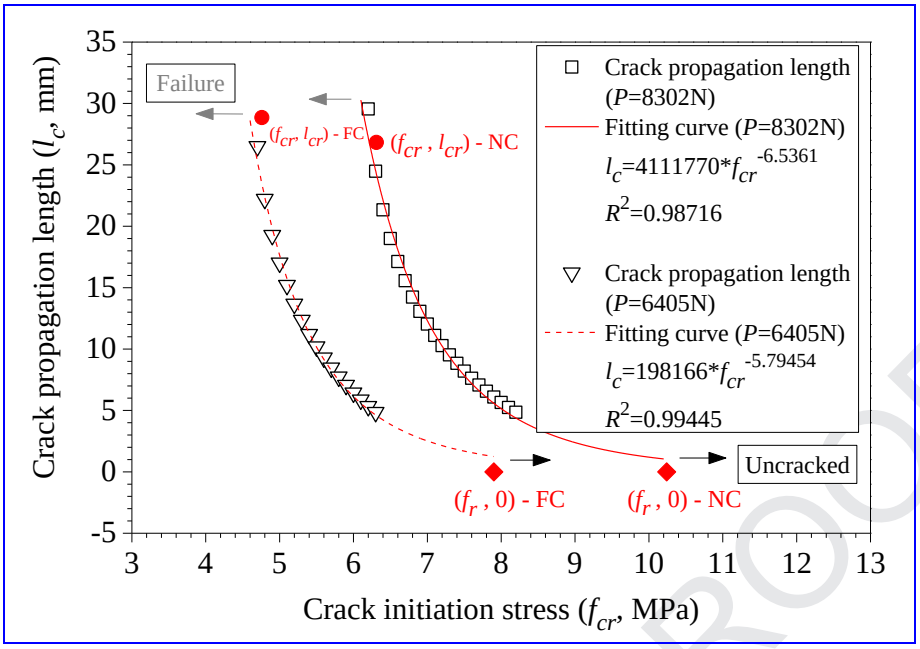

Fig. 13. The relationship between f_{cr} and crack propagation length at certain loads (based on SDT).

It is significant that the crack propagation length is sensitive to the crack initiation stress adopted. With the increase in f_{cr}, the crack propagation length reduces quickly. This trend agrees with the fact that, for the specimen with a higher crack initiation stress, it can bear a higher load with the potential extra crack propagation capacity. When the stress is larger than the modulus of rupture, the obtained l_c is nearly equal to 0, which can be regarded as uncracked. For both specimens, the obtained f_{cr-SDT}, 6.31 and 4.71 MPa, are much close to the minimum one in available crack initiation stress (6.1 and 4.7 MPa). It indicates that the adopted trigonometric shear deformation theory can give the stress predictions with high accuracy.

4.5 The relationship of f_r, f_{cr} and f_{spt}

Nominally, the splitting tensile strength is regarded as the crack initiation stress in the softening model. The rationale of this assumption is analysed below.

The relationship between the modulus of rupture (f_r) and compressive strength, the splitting tensile strength (f_{spt}) and compressive strength have been studied comprehensively for prediction purpose. The ACI Code [47] defines the modulus of rupture and splitting tensile stress as $f_r = 0.7 f_c^{1/2}$ and $f_{spt} = 0.56 f_c^{1/2}$. Similarly, $f_r = 0.3 f_c^{0.67}$ and $f_{spt} = 0.3 f_c^{2/3}$ are adopted in the Euro Code [48] and CEB-FIP [49] respectively. Based on

statistical study and support vector machine learning theory, $f_r = 0.7 f_c^{1/2}$ and $f_{spt} = 0.283 f_c^{0.681}$ are proposed by F. Legeron et al. [50] and A. Behnood et al. [51] respectively. In contrast, there is limited research focused on the relation between f_r and f_{spt}.

The experimental results of f_r and f_{spt} in mechanical properties studies [52–59] are introduced for analysis. All the test results are presented in Fig. 14. The relationships obtained from the code [47–49] and the previous studies [50,51] are also plotted. As shown in Fig. 14, $f_r = f_{spt}$ is the lower bound relationship, and $f_r = 1.25 f_{spt}$ is close to the average. The relationship, $f_r = 2.3761 f_{spt}^{0.7342}$, obtained from [50] and [51], is more likely to overestimate the modulus of rupture. Hence, a fitting equation, $f_r = 1.1578 f_{spt}^{1.0921}$, is proposed for reference in the concrete fracture analysis.

The above comparison indicates that the modulus of rupture is about 1.25 times of the splitting tensile. For the crack initiation stress, f_{cr}, it may be 12.5 percent larger than the f_{spt}. As the crack propagation length is very sensitive to the crack initiation stress, this difference cannot be neglected in the fracture calculations.

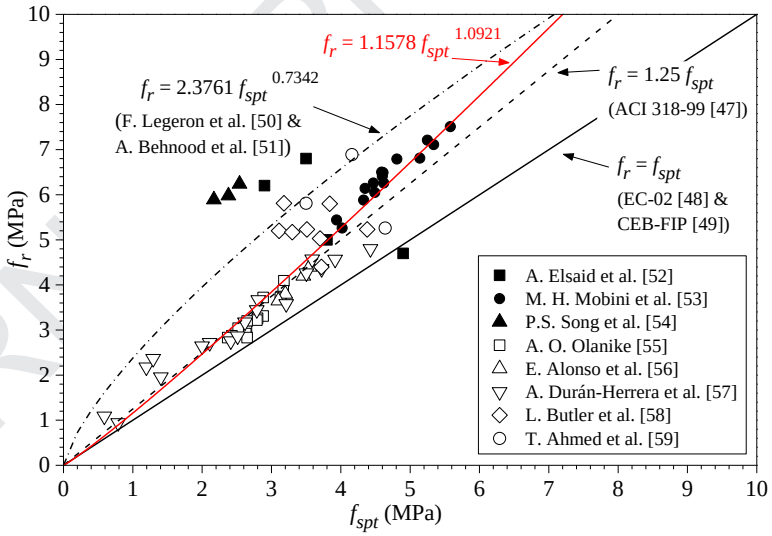

Fig. 14. The relationship between f_{spt} and f_r.

5. Conclusions

In this study, the trigonometric shear deformation theory has been developed to analyse concrete beams in TPBT. The crack initiation stress, modulus of rupture, elastic modulus and critical crack propagation length are

considered. Fracture tests of notched beams were designed to validate the accuracy of the theory developed. Based on the outputs, the following conclusions can be drawn:

(1) For the commonly adopted specimens with a span to depth ratio of 3 in flexural strength test, the modulus of rupture obtained with SDT is nearly 1.5 times of that obtained with CBT in the ASTM, British and European codes [28–30]. The crack initiation stress, i.e. the maximum nominal stress in the crack tip, is about 90% of the modulus of rupture provided by the ASTM, British and European codes [28–30].

(2) For the notched concrete beams in TPBT with a span to depth ratio of 3 and 4, the proposed equation can provide accurate results of elastic modulus. The difference is within 3% between the calculated and the measured values in this study.

(3) The crack initiation stress is about 1.125 times of the splitting tensile strength. In the crack and fracture calculations of concrete materials, it may not be appropriate to adopt the splitting tensile strength as the crack initiation stress.

(4) The computed crack propagation length is in a good agreement with the DIC results. This indicates that the stress distribution based on SDT is more reasonable than the CBT one.

Acknowledgement

The authors are sincerely grateful for the financial support provided by the National Natural Science Foundation of China (No. 11832007, 11572057 & 51408382) and the Science & Technology Support Program of Sichuan Province (No. 2016HH0037). The first author is supported by the China Scholarship Council (CSC) for the visiting to University of Liverpool, which is sincerely appreciated.

References

[1] Ghourchian S, Wyrzykowski M, Baquerizo L, Lura P. Performance of passive methods in plastic shrinkage cracking mitigation. Cem Concr Compos 2018;91:148–55. doi:10.1016/j.cemconcomp.2018.05.008.

[2] Shields Y, Garboczi E, Weiss J, Farnam Y. Freeze-thaw crack determination in cementitious materials using 3D X-ray computed tomography and acoustic emission. Cem Concr Compos 2018;89:120–9. doi:10.1016/j.cemconcomp.2018.03.004.

[3] Suleiman AR, Nehdi ML. Effect of environmental exposure on autogenous self-healing of cracked cement-based materials. Cem Concr Res 2018;111:197–208. doi:10.1016/j.cemconres.2018.05.009.

[4] Wang X, Fang C, Li D, Han N, Xing F. A self-healing cementitious composite with mineral admixtures and

built-in carbonate. Cem Concr Compos 2018;92:216–29. doi:10.1016/j.cemconcomp.2018.05.013.
[5] De Belie N, Gruyaert E, Al-Tabbaa A, Antonaci P, Baera C, Bajare D, et al. A Review of Self-Healing Concrete for Damage Management of Structures. Adv Mater Interfaces 2018;5:1–28. doi:10.1002/admi.201800074.
[6] Wang JY, Guo JY. Damage investigation of ultra high performance concrete under direct tensile test using acoustic emission techniques. Cem Concr Compos 2018;88:17–28. doi:10.1016/j.cemconcomp.2018.01.007.
[7] Hassan AMT, Jones SW, Mahmud GH. Experimental test methods to determine the uniaxial tensile and compressive behaviour of Ultra High Performance Fibre Reinforced Concrete(UHPFRC). Constr Build Mater 2012;37:874–82. doi:10.1016/j.conbuildmat.2012.04.030.
[8] Li VC, Wu H-C, Maalej M, Mishra DK, Hashida T. Tensile Behavior of Cement-Based Composites with Random Discontinuous Steel Fibers. J Am Ceram Soc 1996;79:74–8. doi:10.1111/j.1151-2916.1996.tb07882.x.
[9] Barragán BE, Gettu R, Martín MA, Zerbino RL. Uniaxial tension test for steel fibre reinforced concrete - A parametric study. Cem Concr Compos 2003;25:767–77. doi:10.1016/S0958-9465(02)00096-3.
[10] Roth M, Eamon C, Slawson T, Tonyan T, Dubey A. Ultra-high-strength, glass fiber-reinforced concrete: Mechanical behavior and numerical modeling. ACI Mater J 2010;107:185.
[11] Swaddiwudhipong S, Lu HR, Wee TH. Direct tension test and tensile strain capacity of concrete at early age. Cem Concr Res 2003;33:2077–84. doi:10.1016/S0008-8846(03)00231-X.
[12] Wille K, El-Tawil S, Naaman AE. Properties of strain hardening ultra high performance fiber reinforced concrete (UHP-FRC) under direct tensile loading. Cem Concr Compos 2014;48:53–66. doi:10.1016/j.cemconcomp.2013.12.015.
[13] Kumar S, Barai S V. Concrete Fracture Models and Applications. Berlin, Heidelberg: Springer Berlin Heidelberg; 2011. doi:10.1007/978-3-642-16764-5.
[14] Xu S, Zhang X. Determination of fracture parameters for crack propagation in concrete using an energy approach. Eng Fract Mech 2008;75:4292–308. doi:10.1016/j.engfracmech.2008.04.022.
[15] Canteli AF, Castanon-Jano L, Cifuentes H, Muñiz-Calvente M, Castillo E. Fitting the fracture curve of concrete as a density function pertaining to the generalized extreme value family. Mater Des 2017;129:201–9. doi:10.1016/j.matdes.2017.05.030.
[16] Zhao Z, Kwon SH, Shah SP. Effect of specimen size on fracture energy and softening curve of concrete: Part I. Experiments and fracture energy. Cem Concr Res 2008;38:1049–60. doi:10.1016/j.cemconres.2008.03.017.
[17] Lee J, Lopez MM. An Experimental Study on Fracture Energy of Plain Concrete. Int J Concr Struct Mater 2014;8:129–39. doi:10.1007/s40069-014-0068-1.
[18] Ma Z, Zhao T, Yang J. Fracture Behavior of Concrete Exposed to the Freeze-Thaw Environment. J Mater Civ Eng 2017;29. doi:10.1061/(ASCE)MT.1943-5533.0001901.
[19] Kumar S, Barai S V. Determining the double-K fracture parameters for three-point bending notched concrete beams using weight function. Fatigue Fract Eng Mater Struct 2010;33:645–60. doi:10.1111/j.1460-2695.2010.01477.x.
[20] Chen Y, Wang K, Wang X, Zhou W. Strength, fracture and fatigue of pervious concrete. Constr Build Mater 2013;42:97–104. doi:10.1016/j.conbuildmat.2013.01.006.
[21] Pradhan S, Kumar S, Barai S V. Recycled aggregate concrete: Particle Packing Method (PPM) of mix design approach. Constr Build Mater 2017;152:269–84. doi:10.1016/j.conbuildmat.2017.06.171.
[22] Mobasher B, Bakhshi M, Barsby C. Backcalculation of residual tensile strength of regular and high performance fiber reinforced concrete from flexural tests. Constr Build Mater 2014;70:243–53. doi:10.1016/j.conbuildmat.2014.07.037.
[23] Brake NA, Allahdadi H, Adam F. Flexural strength and fracture size effects of pervious concrete. Constr Build Mater 2016;113:536–43. doi:10.1016/j.conbuildmat.2016.03.045.
[24] Carpinteri A, Chiaia B, Ferro G. A new explanation for size effects on the flexural strength of concrete. Mag Concr Res 1997;49:45–53. doi:10.1680/macr.1997.49.178.45.
[25] Hibbeler RC, Yap KB. Mechanics of materials. 10th ed. Harlow, England : Pearson Education; 2018.
[26] Tada H, Paris PC, Irwin GR. The Stress Analysis of Cracks Handbook. vol. 11. 2000.
[27] Shah SP. Determination of fracture parameters (K(Formula presented.) and CTODc) of plain concrete using three-point bend tests. Mater Struct Matériaux Constr 1990;23:457–60. doi:10.1007/BF02472029.
[28] ASTM. Standard Test Method for Flexural Strength of Concrete (Using Simple Beam With Center-Point Loading). C293/C293M-16 2016.
[29] BS, EN. 12390-5. Testing hardened concrete--Part 5: flexural strength of test specimens. Br Stand Institution-BSI CEN Eur Comm Stand 2009.
[30] European S. DRAFT pr EN 12390-5:2017 E. Testing hardened concrete - Part 5: Flexural strength of test specimens. Br Stand Institution-BSI CEN Eur Comm Stand 2017.

[31] Mantari JL, Oktem AS, Guedes Soares C. A new trigonometric shear deformation theory for isotropic, laminated composite and sandwich plates. Int J Solids Struct 2012;49:43–53. doi:10.1016/j.ijsolstr.2011.09.008.
[32] Arya H, Shimpi RP, Naik NK. A zigzag model for laminated composite beams. Compos Struct 2002;56:21–4. doi:10.1016/S0263-8223(01)00178-7.
[33] Mantari JL, Oktem AS, Guedes Soares C. Static and dynamic analysis of laminated composite and sandwich plates and shells by using a new higher-order shear deformation theory. Compos Struct 2011;94:37–49. doi:10.1016/j.compstruct.2011.07.020.
[34] Kulkarni K, Singh BN, Maiti DK. Analytical solution for bending and buckling analysis of functionally graded plates using inverse trigonometric shear deformation theory. Compos Struct 2015;134:147–57. doi:10.1016/j.compstruct.2015.08.060.
[35] Farzam-Rad SA, Hassani B, Karamodin A. Isogeometric analysis of functionally graded plates using a new quasi-3D shear deformation theory based on physical neutral surface. Compos Part B Eng 2017;108:174–89. doi:10.1016/j.compositesb.2016.09.029.
[36] Shimpi RP, Ghugal YM. A new layerwise trigonometric shear deformation theory for two-layered cross-ply beams. Compos Sci Technol 2001;61:1271–83. doi:10.1016/S0266-3538(01)00024-0.
[37] Viola E, Tornabene F, Fantuzzi N. General higher-order shear deformation theories for the free vibration analysis of completely doubly-curved laminated shells and panels. Compos Struct 2013;95:639–66. doi:10.1016/j.compstruct.2012.08.005.
[38] Mantari JL, Guedes Soares C. Bending analysis of thick exponentially graded plates using a new trigonometric higher order shear deformation theory. Compos Struct 2012;94:1991–2000. doi:10.1016/j.compstruct.2012.01.005.
[39] Ferreira AJM, Roque CMC, Jorge RMN. Analysis of composite plates by trigonometric shear deformation theory and multiquadrics. Comput Struct 2005;83:2225–37. doi:10.1016/j.compstruc.2005.04.002.
[40] Zenkour AM. Generalized shear deformation theory for bending analysis of functionally graded plates. Appl Math Model 2006;30:67–84. doi:10.1016/j.apm.2005.03.009.
[41] Tounsi A, Houari MSA, Benyoucef S, Adda Bedia EA. A refined trigonometric shear deformation theory for thermoelastic bending of functionally graded sandwich plates. Aerosp Sci Technol 2013;24:209–20. doi:10.1016/j.ast.2011.11.009.
[42] Underwood JH, Kapp JA. More on compliance of the 3-point bend. Int J Fract 1985;28:R41–5.
[43] Wu S-X. Fracture toughness determination of bearing steel using chevron-notch three point bend specimen. Eng Fract Mech 1984;19:221–32. doi:10.1016/0013-7944(84)90017-1.
[44] Guinea G V., Pastor JY, Planas J, Elices M. Stress intensity factor, compliance and CMOD for a general three-point-bend beam. Int J Fract 1998;89:103–16. doi:10.1023/A:1007498132504.
[45] Zhang D, Wu K. Fracture process zone of notched three-point-bending concrete beams. Cem Concr Res 1999;29:1887–92. doi:10.1016/S0008-8846(99)00186-6.
[46] Guo M, Alam SY, Bendimerad AZ, Grondin F, Rozière E, Loukili A. Fracture process zone characteristics and identification of the micro-fracture phases in recycled concrete. Eng Fract Mech 2017;181:101–15. doi:10.1016/j.engfracmech.2017.07.004.
[47] Cagley JR, Barnes CE. Building Code Requirements for Structural Concrete (ACI 318-99) and Commentary (ACI 318R-99). American: 1999.
[48] Beeby AW, Narayanan RS, Narayanan R. Designers' Handbook to Eurocode 2: 1. Design of concrete structures. Thomas Telford; 1995.
[49] Evaluation of the Time Dependent Behaviour of Concrete. Bulletin d'Information No. 199. Lausanne: Comite European du Béton/Fédération Internationale de la Precontrainte; 1991.
[50] Légeron F, Paultre P. Prediction of Modulus of Rupture of Concrete. ACI Mater J 2000;97:193–200. doi:10.14359/823.
[51] Behnood A, Verian KP, Modiri Gharehveran M. Evaluation of the splitting tensile strength in plain and steel fiber-reinforced concrete based on the compressive strength. Constr Build Mater 2015;98:519–29. doi:10.1016/j.conbuildmat.2015.08.124.
[52] Elsaid A, Dawood M, Seracino R, Bobko C. Mechanical properties of kenaf fiber reinforced concrete. Constr Build Mater 2011;25:1991–2001. doi:10.1016/j.conbuildmat.2010.11.052.
[53] Mobini MH, Khaloo A, Hosseini P, Esrafili A. Mechanical properties of fiber-reinforced high-performance concrete incorporating pyrogenic nanosilica with different surface areas. Constr Build Mater 2015;101:130–40. doi:10.1016/j.conbuildmat.2015.10.032.
[54] Song PS, Hwang S, Sheu BC. Strength properties of nylon- and polypropylene-fiber-reinforced concretes. Cem Concr Res 2005;35:1546–50. doi:10.1016/j.cemconres.2004.06.033.
[55] Olanike AO. A Comparative Analysis of Modulus of Rupture and Splitting Tensile Strength of Recycled Aggregate Concrete. Am J Eng Res 2014;2:141–7.

[56] Alonso E, Martínez L, Martínez W, Villaseñor L. Mechanical properties of concrete elaborated with igneous aggregates. Cem Concr Res 2002;32:317–21. doi:10.1016/S0008-8846(01)00655-X.
[57] Durán-Herrera A, Juárez CA, Valdez P, Bentz DP. Evaluation of sustainable high-volume fly ash concretes. Cem Concr Compos 2011;33:39–45. doi:10.1016/j.cemconcomp.2010.09.020.
[58] Butler L, West JS, Tighe SL. Effect of recycled concrete coarse aggregate from multiple sources on the hardened properties of concrete with equivalent compressive strength. Constr Build Mater 2013;47:1292–301. doi:10.1016/j.conbuildmat.2013.05.074.
[59] Ahmed T, Burley E, Rigden S, Abu-Tair AI. The effect of alkali reactivity on the mechanical properties of concrete. Constr Build Mater 2003;17:123–144. doi:https://doi.org/10.1016/S0950-0618(02)00009-0.

Appendix

A. The computed coefficients in W_m and X_m

For specimen with a span of *l* and a depth of *h*, the coefficients in W_m and X_m are as follows.

$$\begin{aligned}
A_1 &= 609352794144333891512279364585672 \\
B_1 &= 2778046668940015 \\
C_1 &= 562949953421312 \\
D_1 &= 705337708325815602159477997042624411267456860 45 \\
G_1 &= 206760185653755264372406867439246885494194176 \\
A_2 &= 436765889032398006375275097303035385987433758720
\end{aligned} \tag{A.1}$$

B. The relationship between g_1, g_2 and h

For beams with a span of 300 mm but different depths, the calculated results of g_1 and g_2 at mid-span are shown in Fig. B1. It is obvious that both g_1 and g_2 have a good exponential relationship with the depth of *h*. And they can be expressed as $g_i = \alpha_i \cdot h^{\beta_i}$, where *i* equals to 1 and 2 respectively.

JOURNAL PRE-PROOF

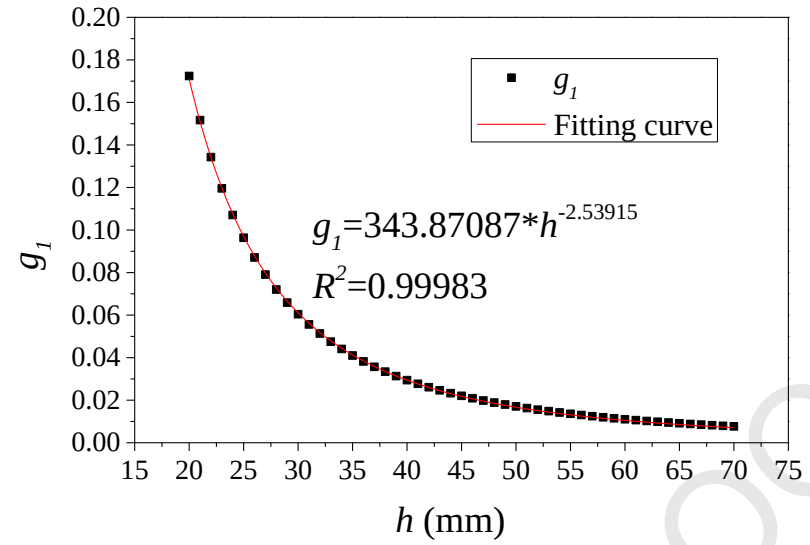

(a)

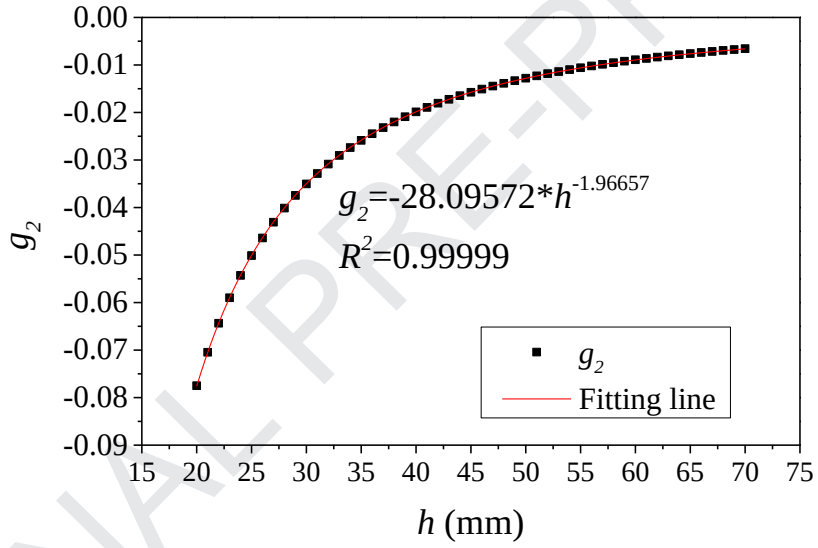

(b)

Fig. B.1. The fitting curves of g_1 and g_2.

For beam with a span of 400 mm and consideration of the mid-span cross-section, the coefficients in Eq. B1 are $\alpha_1 = 500.11912$, $\beta_1 = -2.60045$, $\alpha_2 = -26.91994$ and $\beta_2 = -1.95765$. The R-Square is 0.99981 and 0.99999 respectively.

JOURNAL PRE-PROOF

JOURNAL PRE-PROOF

Highlights:

- Shear deformation theory was adopted to analyse the stress distribution in TPBT.
- Crack initiation stress is about 90% of the modulus of rupture.
- Crack initiation stress is about 1.125 times the tensile strength.
- Elastic modulus and ultimate crack length can be accurately calculated based on SDT.

JOURNAL PRE-PROOF